ACS OMEGA

http://pubs.acs.org/journal/acsodf

Article

Raman Spectroscopic Characterization of Chemical Bonding and Phase Segregation in Tin (Sn)-Incorporated Ga_2O_3

Debabrata Das, Guillermo Gutierrez, and C. V. Ramana*

Cite This: *ACS Omega* 2023, 8, 11709−11716

Read Online

ACCESS | Metrics & More | Article Recommendations

ABSTRACT: Using detailed Raman scattering analyses, the effect of tin (Sn) incorporation on the crystal structure, chemical bonding/inhomogeneity, and single-phase versus multiphase formation of gallium oxide (Ga_2O_3) compounds is reported. The Raman characterization of the Sn-mixed Ga_2O_3 polycrystalline compounds ($0.00 \leq x \leq 0.30$), which were produced by the high-temperature solid-state synthesis method, indicated that the Sn-induced changes in the chemical bonding and phase segregation were significant. Furthermore, the evolution of Sn−O bonds with increasing Sn concentration (x) was confirmed. While the monoclinic β-Ga_2O_3 was unperturbed for lower x values, Raman spectra revealed the nucleation of a composite with a distinct SnO_2 secondary phase. A higher Sn content led to the formation of a Ga−Sn−O + SnO_2 mixed phase compound, which was reflected in shifts in the high-frequency stretching and bending of the GaO_4 tetrahedra that structurally formed the β-Ga_2O_3 phase. Thus, a chemical composition/phase/chemical bonding correlation was established for the Sn-incorporated Ga_2O_3 compounds.

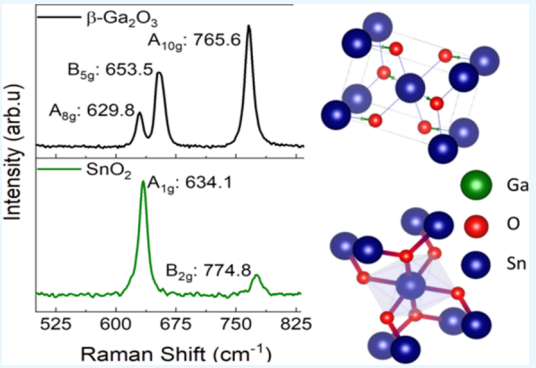

INTRODUCTION

Wide-band-gap gallium oxide (Ga_2O_3) has interesting structural, physical, and chemical properties that make it useful in various modern and future technological contexts.[1−15] Numerous fields of science and technology applications, such as electronics, optoelectronics, photonics, neuromorphic, energy storage and conversion, catalysis, and chemical sensors, can consider integrating Ga_2O_3 and Ga_2O_3-based alloys. Deep-ultraviolet photodetectors, high-power electronics, field-effect transistors, sensors, liquid eutectic contacts, solar cells, cost-efficient light-emitting diodes, and catalysts are just some of the devices that could benefit from the use of these materials.[1,3,7,10−13,15−19]

Ga_2O_3 is appealing for use in solid-state power electronic and optoelectronic devices due to its superior thermodynamic stability and ultrawide band gap (~4.8 eV).[3,7,10,11,16] When compared to other TCOs like In_2O_3, SnO_2, r-GeO_2, and ZnO, Ga_2O_3 has an even larger band gap. Recent research and development efforts have focused on β-Ga_2O_3, suggesting that it might replace the conventional SiC and GaN power devices used in high-voltage applications.[3,10,20] Ga_2O_3 is also an intriguing material from a fundamental scientific standpoint, exhibiting six individual polymorphs, namely, the α, β, γ, δ, ε, and κ phases.[21,22] β-Ga_2O_3, which crystallizes in a monoclinic crystal structure of the C2/m/C32h space group, demonstrates exceedingly high and favorable chemical and thermal stabilities in contrast to other polymorphs.[20]

In recent years, β-Ga_2O_3 and alloys or composites based on β-Ga_2O_3 have garnered considerable attention in experimental and theoretical investigations. Advancements in the field have been made as a result of efforts to comprehend the impact of various metal ions in β-Ga_2O_3. For instance, Si-doped Ga_2O_3 dramatically improved the electrical conductivity because Si^{4+} acted as a donor impurity and increased the electron concentration drastically.[23,24] The formation energy and defect structure of various transition-metal (TM) ions incorporated into β-Ga_2O_3 have been the subject of theoretical studies, which have proven to be extremely helpful.[25,26] Furthermore, it was shown that the chemistry of particular ions can significantly affect the efficiency of photocatalysis and electrochemistry for energy storage.[15,27] A sufficient number of studies have also been done on the material's optical and optoelectronic characteristics. It has been reported that by manipulating the shape of nanocrystals and incorporating rare-earth ions into Ga_2O_3 nanomaterials, a wide range of photoluminescence properties can be achieved.[6,16,28] The optical band gap was considerably narrowed and shifted to

Received: August 7, 2022
Accepted: November 21, 2022
Published: March 22, 2023

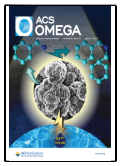

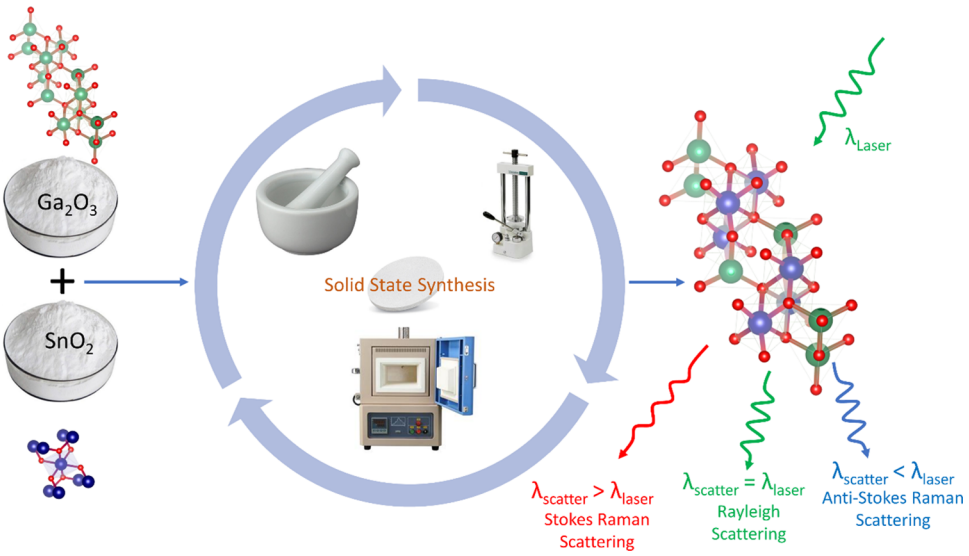

Figure 1. Schematic representation of the conceptual layout of the present work employed for synthesis and structural characterization of Ga−Sn−O samples. Starting from left to right, the schematic diagram represents the mixing of respective oxides, the solid-state synthesis procedure employed, and the principle of Raman spectroscopic characterization to evaluate the structure and chemical bonding of Ga−Sn−O samples. The images shown are taken at the CMR, Materials Synthesis Laboratory, and created by the team of authors.

the red by adding TM ions like Fe, Ti, and W into β-Ga_2O_3.[12,29−31] Exploring the science of Sn-incorporation into Ga_2O_3 and enlightening the phase-structure−property correlations are advantageous not only from a core crystallographic perspective but also for extracting novel properties and phenomena, which can aid in the design of materials for sophisticated electronic and optoelectronic devices.

In recent years, there has been considerable interest in the prospect of doping or alloying Ga_2O_3 with tin.[15,32−37] Using the float zone method, Sn-doped Ga_2O_3 single crystals were grown, and it was shown that the electrical resistivity and carrier concentration could be adjusted by controlling the amount of Sn doped into the material. Sn-doped Ga_2O_3 thin films with n-type conductivity and a carrier concentration of 1.95×10^{17} cm^{-3} were deposited using metal−organic chemical vapor deposition. The photocatalytic activity of Sn-intermixed (0.7 atom %) β-Ga_2O_3 nanostructures was found to be significantly higher than that of intrinsic β-Ga_2O_3. These findings suggest novel avenues for establishing extremely efficient photocatalysts based on β-Ga_2O_3 for use in fields such as environmental cleanup, germ killing, and targeted chemical reactions.[35] However, even though Sn incorporation into β-Ga_2O_3 single crystals and thin films has been extensively explored in recent years, the fundamental aspects of Sn-mixing in Ga_2O_3 inorganic compounds have received little attention in the literature.

A deeper understanding of the crystal structure, electronic structure, and structure−property correlation is critical to manipulating the material for desired applications. Therefore, we employed Raman spectroscopy, an effective and non-destructive technique to probe materials' structure and chemical bonding at all length scales,[38−40] to gain deeper insight into the crystal structure and chemical bonding in Sn-assimilated Ga_2O_3 compounds. Furthermore, Raman spectroscopy allows for determining the presence of even noncrystalline secondary phases, which may not appear in traditional X-ray diffraction measurements.[38,39] Interestingly, as presented and discussed in this contribution, Raman scattering analyses allowed us to identify features of the core internal structure and chemical bonding in Sn-incorporated Ga_2O_3, as well as differentiate the presence of a single phase versus a composite formation (Figure 1).

EXPERIMENTAL DETAILS

A high-temperature solid-state chemical process was used to synthesize Ga−Sn−O materials. Pure powders of Ga_2O_3 (99.99%, product no. 215066) and SnO_2 (99.99%, product no. 204714) from Sigma Aldrich were blended entirely together to produce a series of Sn-mixed Ga_2O_3 compounds. According to the chemical formula $(Ga_{1-x}Sn_x)_2O_3$, where x is the atomic percentage of Sn introduced, the ratio for Sn was adjusted based on balanced stoichiometry. Sn concentrations between $x = 0.0$ and $x = 0.3$ were used to produce the materials. We started the solid-state synthesis technique by grinding the powders with a mortar and pestle in a volatile liquid environment, resulting in uniform mixing and creating particles with ever smaller dimensions. This resulted in uniform mixing and creating particles with ever smaller dimensions. Then, the mixed compound was calcined at 1100 °C for 12 h. Both the heating and cooling ramp rates were set at 5 °C/min. After calcination, the sample was pulverized using polyvinyl acetate, followed by pressing into pellets of 8 mm diameter and 2 mm thickness. The final step of the Sn-mixed Ga_2O_3 synthesis involved a sintering process. The goal was to make a reasonably dense material by narrowing the powder particles' pores and getting rid of any other flaws that might have been there. The sintering temperature was set to 1350 °C for 12 h while retaining the same ramp rate. This process yielded Sn-mixed Ga_2O_3 materials with varying Sn concentrations (x), which were characterized for insights into their structure−composition relation. The fabrication processes for making pure Ga_2O_3 and SnO_2 pellets were identical.

A micro-Raman (Renishaw) spectrophotometer with 532 nm laser excitation was used for Raman spectroscopy. As published extensively in the literature, standard methods were used to fit the peaks.[41] Briefly, Raman spectra were fitted by a superposition of the Lorentzian function:[41]

https://doi.org/10.1021/acsomega.2c05047
ACS Omega 2023, 8, 11709−11716

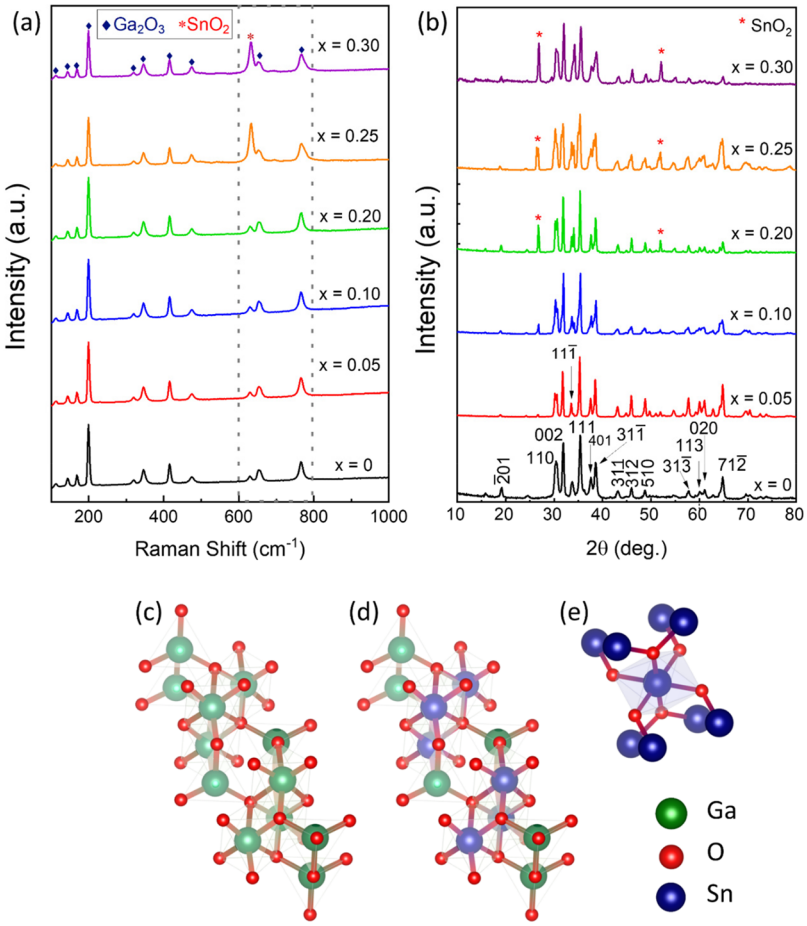

Figure 2. (a) Raman spectroscopy and (b) XRD [reprinted (adapted) with permission from ref 45. Copyright 2022 American Chemical Society] data of Ga−Sn−O compounds with varying Sn concentrations, $x = 0.00$ to $x = 0.30$. (c) Schematic of pure monoclinic β-Ga_2O_3 crystal structure. (d) Schematic of mixed $(Ga_{1-x}Sn_x)_2O_3$ monoclinic crystal structure with partial substitutional replacement of Ga atoms by Sn. (e) Schematic of pure rutile SnO_2 crystal structure.

$$I(\omega) = I_0 + \left(\frac{2A}{\pi}\right)\left(\frac{W}{W + 4(\omega - \omega_0)^2}\right) \quad (1)$$

where ω, ω_0, W, A, and I_0 are the peak phonon frequency, maximum peak phonon frequency, full width at half maxima (FWHM), normalization constant, and background intensity, respectively.

RESULTS AND DISCUSSION

The Raman spectroscopic and X-ray diffraction (XRD) data of the Sn-incorporated Ga_2O_3 samples are shown in Figure 2a,b, where the data shown are for various concentrations of Sn (x). Figure 2c−e depicts three possible phases present in the solid solution. The Raman peaks observed for all concentrations of Sn remained the same for each value of x. The Raman peaks observed were approximately located at 112, 143, 169, 199, 320, 346, 415, 475, 630, 654, and 766 cm^{-1}, which corresponded to A_{1g}, B_{2g}, A_{2g}, A_{3g}, A_{4g}, A_{5g}, A_{6g}, A_{7g}, A_{8g}, B_{5g}, and A_{10g}, vibrations, respectively.[42] The lower frequency bands at 112, 143, 169, and 199 cm^{-1} were assigned to the translations and vibrations of chains, while the bands at 320, 346, and 415 cm^{-1} were assigned to the deformation of the octahedron.[42] The higher frequency bands at 475, 630, 654, and 766 cm^{-1} were assigned to the bending and stretching of the tetrahedron.[42] All peak positions and mode assignments agreed well with those reported for bulk β-Ga_2O_3.

The Raman spectra were analyzed for crystal structure and crystal symmetry to further understand the chemical purity and bonding within Ga−Sn−O. For $x = 0.0$, the sample exhibits the characteristic Raman peaks related to intrinsic monoclinic β-Ga_2O_3.[43,44] As Sn concentration increases, the Raman data show the peak evolution and intensity variation, which is fully dependent on the Sn-content. It appears that a secondary Sn-alloyed β-Ga_2O_3 phase (Ga−Sn−O) forms, where Ga atoms are partially substituted by Sn atoms, while Ga−Sn−O + SnO_2 composite formation occurs at higher values of Sn(x). Also, the XRD peaks[45] (Figure 2b) for $x \leq 0.1$ are identified and indexed to the phase pure monoclinic β-Ga_2O_3 phase. For $x \geq 0.2$, peaks corresponding to the tetragonal SnO_2 phase start evolving. We have used a high-temperature solid-state process during the fabrication of Sn-incorporated Ga_2O_3 compounds, where the solubility limit is slightly higher due to the high-temperature processing. However, Wang et al.[36] and Ryou et al.[35,36] have independently reported, based on different studies, a relatively lower solubility limit, which may be primarily due to the lower processing temperature adopted. Detailed Rietveld analysis,[45] along with the findings from Raman scattering of corresponding samples, supports that the Sn incorporation induces a secondary phase formation with an increasing concentration of $x \geq 0.20$. Additional structural and optical characterization of Sn-incorporated Ga_2O_3 compounds, which was reported earlier, has followed the same trend.[37,45]

https://doi.org/10.1021/acsomega.2c05047
ACS Omega 2023, 8, 11709−11716

The peak positions corresponding to active Raman modes, as shown in Figure 2a, are listed in Table 1 with their

Table 1. Peak Position (in cm^{-1}) of Active Raman Vibration Modes in $(Ga_{1-x}Sn_x)_2O_3$ Compounds with Increasing Sn Concentration from $x = 0.00$ to $x = 0.30$

Raman modes	$x = 0.00$	$x = 0.05$	$x = 0.10$	$x = 0.20$	$x = 0.25$	$x = 0.30$
A_{1g}	112.3	112.3	112.3	112.4	112.1	112.3
B_{2g}	143.6	143.8	143.9	144.0	144.0	143.9
A_{2g}	168.5	168.5	168.6	168.7	168.4	168.4
A_{3g}	199.3	199.3	199.2	199.2	199.2	199.2
A_{4g}	319.4	319.3	319.3	319.3	319.4	319.3
A_{5g}	345.7	345.7	345.8	345.8	345.8	345.7
A_{6g}	415.4	415.4	415.3	415.4	415.4	415.4
A_{7g}	475.0	474.8	474.8	474.2	474.1	474.1
A_{8g}	630.0	630.0	630.0	630.0	632.6	632.5
B_{5g}	653.7	653.7	653.6	653.9	653.4	653.4
A_{10g}	765.9	765.6	765.6	765.9	766.7	766.9

appropriate vibrational symmetry assignments. By identifying the peak positions carefully, the evolution of chemical bonding, intermixing of two different phases, lattice symmetry, and phase segregation in the Sn-incorporated Ga_2O_3 materials can be understood. Until A_{6g} (~415.4 cm^{-1}), there was no significant change in peak position/shape for all values of Sn concentration, and the variation was within ±0.4 cm^{-1}. In contrast, A_{7g} showed a slight frequency shift starting from $x = 0.20$, but the overall peak intensity, shape, and FWHM remained unaffected. However, the last three peaks, A_{8g}, B_{5g}, and A_{10g}, changed dramatically at higher Sn concentrations. Such behavior reflected in the data provided clues about phase identity or the coexistence of phases and can be understood comprehensively by comparing phase-pure β-Ga_2O_3 and SnO_2 Raman spectroscopic data with Sn-mixed Ga_2O_3 compounds in detail.

Figure 3a shows the Raman spectroscopic data of monoclinic β-Ga_2O_3 over a broader spectral range. For clarity and to understand the present data more clearly, the Raman spectrum of a SnO_2 polycrystalline reference sample is also shown (Figure 3a). The spectra can be conveniently used to understand the effect of Sn on the chemical bonding in Ga_2O_3.

Monoclinic β-Ga_2O_3 belongs to the space group C2/m/C32h. Following a factor group analysis,[46] the crystal modes are classified according to

$$\Gamma_{opt} = 10A_g + 5B_g + 4A_u + 8B_u \quad (2)$$

The A_g and B_g symmetries are the Raman-active phonon modes, while those with A_u and B_u are infrared active. A total of 15 Raman modes and 12 infrared active modes were expected for β-Ga_2O_3.[42,46] Rutile SnO_2 of the P42/mnm space group has the following optical vibration modes at the Γ point of the Brillouin zone:[47−50]

$$\Gamma_{opt} = A_{1g} + A_{2g} + A_{2u} + B_{1g} + B_{2g} + 2B_{1u} + E_g + 3E_u \quad (3)$$

Among these, four are Raman active modes, where A_{1g}, B_{1g}, and B_{2g} belong to active nondegenerate modes, and E_g represents an active, doubly degenerate mode. A_{2u} and E_u are infrared active, while A_{2g} and B_{1u} are silent. Only the oxygen atoms vibrate either parallel (doubly degenerate) or perpendicular (nondegenerate) to the *c*-axis. Figure 3c,d shows the oxygen atom vibration modes for A_{1g} and B_{2g}, respectively. These two modes are the most important SnO_2 Raman-active lattice vibration modes for our current study. The $A_{1g}(SnO_2)$ wavenumber is in close proximity to $A_{8g}(\beta$-$Ga_2O_3)$, and that of $B_{2g}(SnO_2)$ is in close proximity to $A_{10g}(\beta$-$Ga_2O_3)$. The relative evolution of these peaks with increasing Sn incorporation, shown in Figure 2a (inside the dotted rectangular box), defines the structural and chemical properties of the Ga−Sn−O composite. $E_g(SnO_2)$ and $A_{7g}(\beta$-$Ga_2O_3)$ also appear at similar wavenumbers. However, insignificant peak modulation (~475 cm^{-1} in Figure 2a) throughout the Sn-incorporated Ga_2O_3 compounds makes the corresponding peak less attractive for further investigation. Figure 3b shows the magnified Raman spectra for both β-Ga_2O_3 and SnO_2, focusing on the four peaks

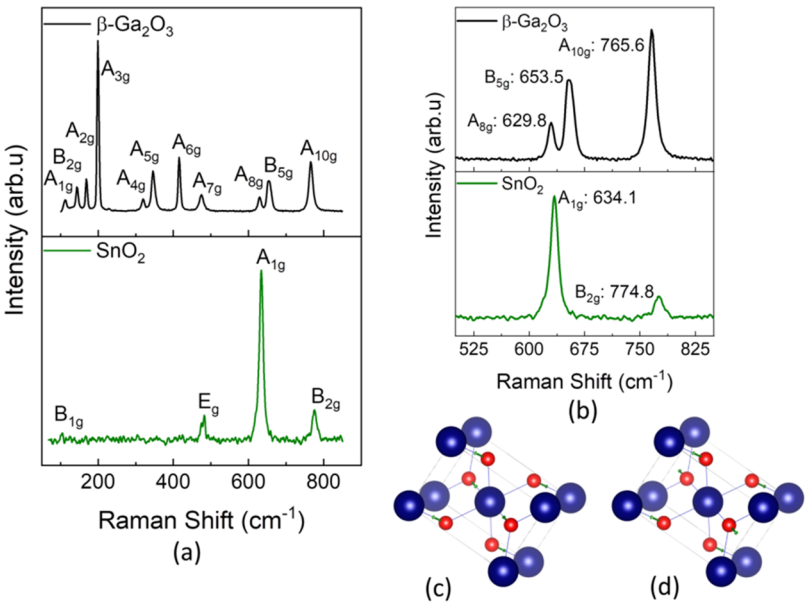

Figure 3. (a) Raman spectra of phase pure β-Ga_2O_3 and SnO_2. (b) Expanded Raman spectra of phase pure β-Ga_2O_3 and SnO_2, indicating $A_{8g}/B_{5g}/A_{10g}$ Raman modes of β-Ga_2O_3 and A_{1g}/B_{2g} of SnO_2. (c, d) Oxygen vibration direction corresponds to A_{1g}/B_{2g} of SnO_2.

https://doi.org/10.1021/acsomega.2c05047
ACS Omega 2023, 8, 11709−11716

as mentioned above. Additionally, the wavenumbers of Raman scattering peaks of phase-pure β-Ga_2O_3 and SnO_2 obtained in the present work, along with mode assignments, are presented in Table 2.

Table 2. Comparison of Raman Peak Positions of Pure β-Ga_2O_3 and SnO_2

Raman modes of β-Ga_2O_3	peak position (cm^{-1})	Raman modes of SnO_2	peak position (cm^{-1})
A_{1g}	112.3	B_{1g}	100.5
B_{2g}	143.6		
A_{2g}	168.5		
A_{3g}	199.3		
A_{4g}	319.4		
A_{5g}	345.7		
A_{6g}	415.4		
A_{7g}	475.0	E_g	479.2
A_{8g}	630.0	A_{1g}	634.2
B_{5g}	653.7		
A_{10g}	765.9	B_{2g}	775.3

Figure 4 highlights the effect of Sn incorporation. The optimized peak fitting was used to extract the active vibrational contributions from the monoclinic and rutile-type phases. The peaks at ~634 and ~774 cm^{-1} correspond to the A_{1g} and B_{2g} bands of rutile SnO_2 (cassiterite phase), respectively.[51] The Sn incorporation did not appear to cause any effect on the overlapped β-Ga_2O_3 peaks (A_{8g} and A_{10g}), such as a shift or broadening/narrowing of the peaks. This confirmed the integrity of the corresponding Raman vibrational mode of the host crystal. It is evident that the SnO_2 peak began to form at a concentration of x = 0.20. A further increase in peak intensity was noted when the Sn concentration was increased to x = 0.30. Deeper insight into the Sn-incorporated Ga_2O_3 chemical stoichiometry can be inferred from this typical behavior seen in the Raman spectroscopic data. Starting from the pure phase β-Ga_2O_3, smaller Sn infusions ($<x$ = 0.20) caused the substitutional replacement of Ga atoms and formed corresponding Ga−Sn−O compounds. The overall lattice structure remained the same, except for the presence of partially Sn-dominated Ga crystallite sites. The fractional coexistence of Sn with the host Ga atoms altered the lattice vibrations slightly, but the overall Raman spectra did not change significantly. Though the monoclinic β-Ga_2O_3 showed active Raman spectra corresponding to mixed Ga/O lattice vibrations, the partial replacement of Ga by Sn did not affect the intrinsic vibrational symmetry considerably. However, at Sn concentrations above x = 0.2, rutile SnO_2 began to form, along with a host-monoclinic Ga−Sn−O phase. The Raman-active lattice vibrations also changed accordingly and became more significant when the Sn concentration was increased to x = 0.30.

The shifts displayed in Table 1 explain the effects due to Sn incorporation. It is evident that the presence of Sn caused a slight change in the Ga−Sn−O Raman-active modes. The evolution of a partially overlapped peak intensity from two different lattice families (β-Ga_2O_3-(A_{8g}/A_{10g}) and SnO_2-(A_{1g}/B_{2g})) is shown in Figure 5a,b. For both cases, the SnO_2/β-Ga_2O_3 ratio increased significantly at Sn concentrations of x = 0.02 and higher. Lower Sn concentrations ($<x$ = 0.20) had a negligible influence on the corresponding Raman peaks, which confirmed the absence of phase segregation. For x < 0.2, Sn has incorporated as a substitutional entity at Ga(II) octahedral sites, and from 20 atomic % onward, it starts forming an additional secondary phase of SnO_2 through interstitial substitution. Varley et al.[25] have clearly shown that Sn always prefers to replace Ga(II) atoms at octahedral lattice sites owing to its lower formation energy. Additionally, there are several reports in the recent literature suggesting the same theoretical prediction.[52,53] Moreover, decreasing peak intensity, related to the mid-frequency range (320, 346, and 415 cm^{-1}), with increasing Sn concentration confirms selective Sn incorporation at Ga_{II}^{3+} sites. But, there is a nominal peak shift observed in such Raman active vibration modes. Yao et al.[52] have reported similar findings, which is due to the localized

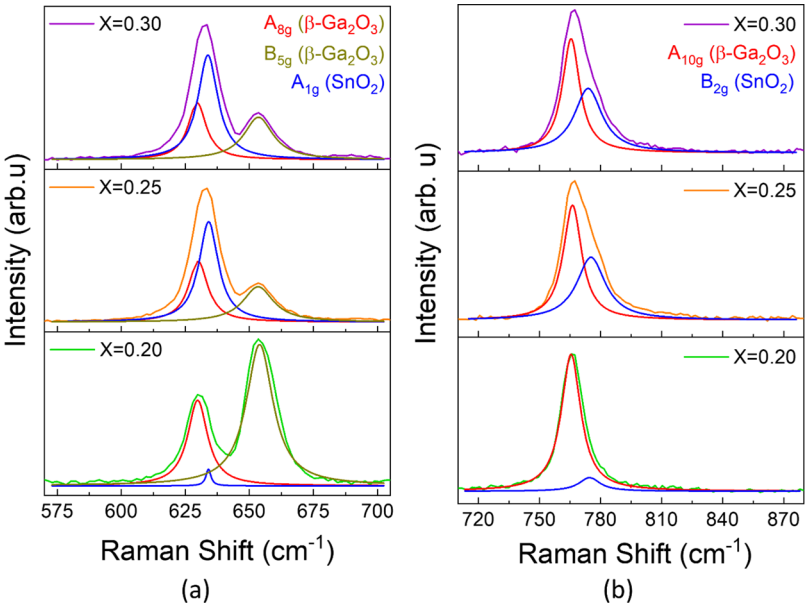

Figure 4. (a, b) Modulation of partially overlapped active Raman peaks of β-Ga_2O_3 (A_{8g}, B_{5g}, and A_{10g}) and SnO_2 (A_{1g}, and B_{2g}) with increasing Sn concentration from x = 0.20 to x = 0.30.

https://doi.org/10.1021/acsomega.2c05047
ACS Omega 2023, 8, 11709−11716

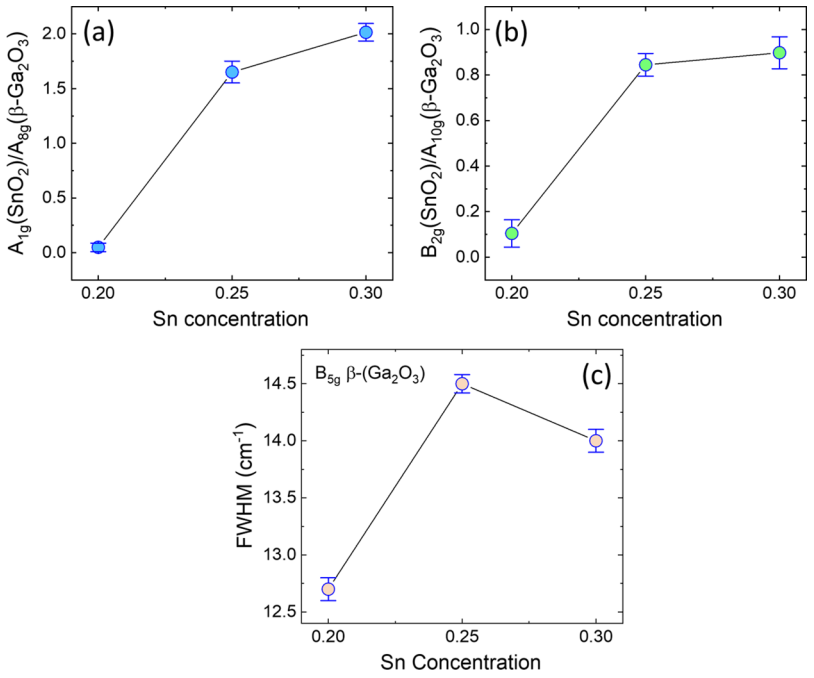

Figure 5. Relative modulation of partially overlapped β-Ga_2O_3 and SnO_2 peaks with increasing concentration of Sn: (a) $A_{1g}(SnO_2)/A_{8g}(\beta\text{-}Ga_2O_3)$ and (b) $B_{2g}(SnO_2)/A_{10g}(\beta\text{-}Ga_2O_3)$. (c) Variation of FWHM of $B_{5g}(\beta\text{-}Ga_2O_3)$ with increasing Sn incorporation.

deformation at octahedral Ga_{II}^{3+} sites than long-range bond stretching. On the contrary, asymmetric tailoring of the Raman active vibrational peaks at a higher frequency range starts appearing from $x \geq 0.2$, where the interstitial accumulation of the SnO_2 phase begins overtaking the Sn incorporation process. Figure 5c highlights another effect of Sn alloying: the broadening of the 653 cm^{-1} peak. At $x = 0.25$ and 0.30, the peak is significantly decreased and broadened. Doping effects on Ga_sO_3 have been reported previously.[41,54] With an increase in dopant comes an increase in the amount of foreign atoms entering the crystal lattice of β-Ga_2O_3, which forms a ternary solid solution.[54] The broadening of the peak at 652 cm^{-1} may be explained by the same principle, as $x = 0.25$ and 0.30 concentration is the threshold amount for solute atoms to enter the lattice. The atomic radii mismatch between Ga^{3+} and Sn^{2+} is large enough to contribute to this peak broadening. Finally, as clearly demonstrated in the present work using Raman spectroscopic studies, the gradual evolution of single-phase Ga−Sn−O versus multiphase Ga−Sn−O + SnO_2 composites with increasing concentration of Sn was also evident in the morphology and microstructure studies, as reported elsewhere.[47]

CONCLUSIONS

Summarizing the results, detailed Raman spectroscopy measurements were performed to characterize the structure, chemical bonding, and phase evolution of Sn-incorporated β-Ga_2O_3. Rutile SnO_2 nucleated and attempted to fuse into the overall structure of the host monoclinic β-Ga_2O_3. Such phase intermixing and composite evolution was perhaps facilitated by thermo-chemical means via solid-state reaction at elevated temperatures. Additionally, the Sn-incorporation concentration, which varied from 0 to 0.3 atomic %, influenced the overall phase composition of the resulting Ga−Sn−O materials. Successful characterization of the relative intrinsic parameters can extract the elementary behavior of the core crystal structure and chemical bonding, as well as differentiate the single-phase versus a composite formation in the $(Ga_{1-x}Sn_x)_2O_3$ materials. These fundamental insights derived from the dopant effect are expected to offer efficient means to design impeccably alloyed, wide-bandgap oxide semiconductors for futuristic electronic, optoelectronic, and photonic devices.

AUTHOR INFORMATION

Corresponding Author

C. V. Ramana − *Center for Advanced Materials Research (CMR) and Department of Mechanical Engineering, University of Texas at El Paso, El Paso, Texas 79968, United States;* orcid.org/0000-0002-5286-3065; Email: rvchintalapalle@utep.edu

Authors

Debabrata Das − *Center for Advanced Materials Research (CMR), University of Texas at El Paso, El Paso, Texas 79968, United States;* orcid.org/0000-0003-4326-6805

Guillermo Gutierrez − *Center for Advanced Materials Research (CMR) and Department of Mechanical Engineering, University of Texas at El Paso, El Paso, Texas 79968, United States*

Complete contact information is available at: https://pubs.acs.org/10.1021/acsomega.2c05047

Notes

The authors declare no competing financial interest.

ACKNOWLEDGMENTS

The authors also acknowledge, with pleasure, support from the National Science Foundation (NSF) with NSF-PREM grant #DMR-1827745. This material is also based upon work supported by the Air Force Office of Scientific Research under award number FA9550-18-1-0387. However, any opinions,

https://doi.org/10.1021/acsomega.2c05047
ACS Omega 2023, 8, 11709−11716

findings, and conclusions or recommendations expressed in this contribution are those of the author(s) and do not necessarily reflect the views of the United States Air Force.

REFERENCES

(1) Zheng, X. Q.; Zhao, H.; Jia, Z.; Tao, X.; Feng, P. X. L. Young's modulus and corresponding orientation in β-Ga_2O_3 thin films resolved by nanomechanical resonators. *Appl. Phys. Lett.* **2021**, *119*, No. 013505.

(2) Kim, H. W.; Lee, J. W.; Kebede, M. A.; Kim, H. S.; Lee, C. Annealing effects of Ga_2O_3−ZnO core-shell heteronanowires. *Mater. Sci. Eng., B* **2009**, *163*, 44−47.

(3) Xia, Z.; Chandrasekar, H.; Moore, W.; Wang, C.; Lee, A. J.; McGlone, J.; Kalarickal, N. K.; Arehart, A.; Ringel, S.; Yang, F.; Rajan, S. Metal/$BaTiO_3$/β-Ga_2O_3 dielectric heterojunction diode with 5.7 MV/cm breakdown field. *Appl. Phys. Lett.* **2019**, *115*, No. 252104.

(4) Wang, D.; Lou, Y.; Wang, R.; Wang, P.; Zheng, X.; Zhang, Y.; Jiang, N. Humidity sensor based on Ga_2O_3 nanorods doped with Na^+ and K^+ from GaN powder. *Ceram. Int.* **2015**, *41*, 14790−14797.

(5) Luo, Y.; Hou, Z.; Gao, J.; Jin, D.; Zheng, X. Synthesis of high crystallization β-Ga_2O_3 micron rods with tunable morphologies and intensive blue emission via solution route. *Mater. Sci. Eng., B* **2007**, *140*, 123−127.

(6) Makeswaran, N.; Das, D.; Zade, V.; Gaurav, P.; Shutthanandan, V.; Tan, S.; Ramana, C. V. Size-and Phase-Controlled Nanometer-Thick β-Ga_2O_3 Films with Green Photoluminescence for Optoelectronic Applications. *ACS Appl. Nano Mater.* **2021**, *4*, 3331−3338.

(7) Kaneko, K.; Fujita, S.; Hitora, T. A power device material of corundum-structured α-Ga_2O_3 fabricated by MIST EPITAXY technique. *Jpn. J. Appl. Phys.* **2018**, *57*, No. 02cb18.

(8) Montedoro, V.; Torres, A.; Dadgostar, S.; Jimenez, J.; Bosi, M.; Parisini, A.; Fornari, R. Cathodoluminescence of undoped and Si-doped ε-Ga_2O_3 films. *Mater. Sci. Eng., B* **2021**, *264*, No. 114918.

(9) Baeissa, E. S.; Mohamed, R. M. Pt/Ga_2O_3−SiO_2 nanoparticles for efficient visible-light photocatalysis. *Ceram. Int.* **2014**, *40*, 841−847.

(10) Zeng, K.; Vaidya, A.; Singisetti, U. A field-plated Ga_2O_3 MOSFET with near 2-kV breakdown voltage and 520 mΩ·cm^2 on-resistance. *Appl. Phys. Express* **2019**, *12*, No. 081003.

(11) Hao, W.; He, Q.; Zhou, K.; Xu, G.; Xiong, W.; Zhou, X.; Jian, G.; Chen, C.; Zhao, X.; Long, S. Low defect density and small I − V curve hysteresis in NiO/β-Ga_2O_3 pn diode with a high PFOM of 0.65 GW/cm^2. *Appl. Phys. Lett.* **2021**, *118*, No. 043501.

(12) Bandi, M.; Zade, V.; Roy, S.; Nair, A. N.; Seacat, S.; Sreenivasan, S.; Shutthanandan, V.; Van de Walle, C. G.; Peelaers, H.; Ramana, C. V. Effect of Titanium Induced Chemical Inhomogeneity on Crystal Structure, Electronic Structure, and Optical Properties of Wide Band Gap Ga_2O_3. *Cryst. Growth Des.* **2020**, *20*, 1422−1433.

(13) Kumar, A.; Bag, A. Ultra-high responsivity (>12.34 kA W^{-1}) of Ga-In bimetallic oxide nanowires based deep-UV photodetector. *Nanotechnology* **2020**, *31*, 304001.

(14) Zhang, Y.; Yan, J.; Li, Q.; Qu, C.; Zhang, L.; Xie, W. Optical and structural properties of Cu-doped β-Ga_2O_3 films. *Mater. Sci. Eng., B* **2011**, *176*, 846−849.

(15) Nair, A. N.; Sanad, M. F.; Jayan, R.; Gutierrez, G.; Ge, Y.; Islam, M. M.; Hernandez-Viezcas, J. A.; Zade, V.; Tripathi, S.; Shutthanandan, V.; Ramana, C. V.; Sreenivasan, T. Lewis Acid Site Assisted Bifunctional Activity of Tin Doped Gallium Oxide and Its Application in Rechargeable Zn-Air Batteries. *Small* **2022**, *18*, No. 2202648.

(16) Farvid, S. S.; Wang, T.; Radovanovic, P. V. Colloidal gallium indium oxide nanocrystals: a multifunctional light-emitting phosphor broadly tunable by alloy composition. *J. Am. Chem. Soc.* **2011**, *133*, 6711−6719.

(17) Yang, L.; Xu, J.; Yuan, K.; Yang, Y.; Sun, J. Highly efficient and stable electroluminescence from Er-doped Ga_2O_3 nanofilms fabricated by atomic layer deposition on silicon. *Appl. Phys. Lett.* **2021**, *118*, 141104.

(18) Kyrtsos, A.; Matsubara, M.; Bellotti, E. On the feasibility of p-type Ga_2O_3. *Appl. Phys. Lett.* **2018**, *112*, No. 032108.

(19) Ahmadi, E.; Koksaldi, O. S.; Zheng, X.; Mates, T.; Oshima, Y.; Mishra, U. K.; Speck, J. S. Demonstration of β-$(Al_xGa_{1-x})_2O_3$/β-Ga_2O_3 modulation doped field-effect transistors with Ge as dopant grown via plasma-assisted molecular beam epitaxy. *Appl. Phys. Express* **2017**, *10*, No. 071101.

(20) Pearton, S. J.; Yang, J.; Cary, P. H.; Ren, F.; Kim, J.; Tadjer, M. J.; Mastro, M. A. A review of Ga_2O_3 materials, processing, and devices. *Appl. Phys. Rev.* **2018**, *5*, No. 011301.

(21) Tak, B. R.; Kumar, S.; Kapoor, A. K.; Wang, D.; Li, X.; Sun, H.; Singh, R. Recent advances in the growth of gallium oxide thin films employing various growth techniques—a review. *J. Phys. D: Appl. Phys.* **2021**, *54*, 453002.

(22) Hou, X.; Zou, Y.; Ding, M.; Qin, Y.; Zhang, Z.; Ma, X.; Tan, P.; Yu, S.; Zhou, X.; Zhao, X.; Xu, G.; Sun, H.; Long, S. Review of polymorphous Ga_2O_3 materials and their solar-blind photodetector applications. *J. Phys. D: Appl. Phys.* **2021**, *54*, No. 043001.

(23) Zhang, F.; Arita, M.; Wang, X.; Chen, Z.; Saito, K.; Tanaka, T.; Nishio, M.; Motooka, T.; Guo, Q. Toward controlling the carrier density of Si doped Ga_2O_3 films by pulsed laser deposition. *Appl. Phys. Lett.* **2016**, *109*, 102105.

(24) Leedy, K. D.; Chabak, K. D.; Vasilyev, V.; Look, D. C.; Mahalingam, K.; Brown, J. L.; Green, A. J.; Bowers, C. T.; Crespo, A.; Thomson, D. B.; Jessen, G. H. Si content variation and influence of deposition atmosphere in homoepitaxial Si-doped β-Ga_2O_3 films by pulsed laser deposition. *APL Mater.* **2018**, *6*, 101102.

(25) Varley, J. B.; Weber, J. R.; Janotti, A.; Van de Walle, C. G. Oxygen vacancies and donor impurities in β-Ga_2O_3. *Appl. Phys. Lett.* **2010**, *97*, 142106.

(26) Peelaers, H.; Lyons, J. L.; Varley, J. B.; Van de Walle, C. G. Deep acceptors and their diffusion in Ga_2O_3. *APL Mater.* **2019**, *7*, No. 022519.

(27) Tatsumi, H.; Teramura, K.; Huang, Z.; Wang, Z.; Asakura, H.; Hosokawa, S.; Tanaka, T. Enhancement of CO Evolution by Modification of Ga_2O_3 with Rare-Earth Elements for the Photocatalytic Conversion of CO_2 by H_2O. *Langmuir* **2017**, *33*, 13929−13935.

(28) Das, D.; Escobar, F. S.; Nalam, P. G.; Bhattacharya, P.; Ramana, C. V. Excitation dependent and time resolved photoluminescence of β-Ga_2O_3, β-$(Ga_{0.955}Al_{0.045})_2O_3$ and β-$(Ga_{0.91}In_{0.09})_2O_3$ epitaxial layers grown by pulsed laser deposition. *J. Lumin.* **2022**, *248*, No. 118960.

(29) Battu, A. K.; Manandhar, S.; Shutthanandan, V.; Ramana, C. V. Controlled optical properties via chemical composition tuning in molybdenum-incorporated β-Ga_2O_3 nanocrystalline films. *Chem. Phys. Lett.* **2017**, *684*, 363−367.

(30) Rubio, E. J.; Ramana, C. V. Tungsten-incorporation induced red-shift in the bandgap of gallium oxide thin films. *Appl. Phys. Lett.* **2013**, *102*, 191913.

(31) Shirsath, S. E.; Wang, D.; Jadhav, S. S.; Mane, M.; Li, S.Ferrites obtained by sol-gel method. In *Handbook of sol-gel science and technology*; Springer Cham: 2018; pp 695−735.

(32) Kawaharamura, T.; Dang, G. T.; Furuta, M. Successful Growth of Conductive Highly Crystalline Sn-Doped α-Ga_2O_3 Thin Films by Fine-Channel Mist Chemical Vapor Deposition. *Jpn. J. Appl. Phys.* **2012**, *51*, No. 040207.

(33) Knight, S.; Mock, A.; Korlacki, R.; Darakchieva, V.; Monemar, B.; Kumagai, Y.; Goto, K.; Higashiwaki, M.; Schubert, M. Electron effective mass in Sn-doped monoclinic single crystal β-gallium oxide determined by mid-infrared optical Hall effect. *Appl. Phys. Lett.* **2018**, *112*, No. 012103.

(34) Galazka, Z.; Irmscher, K.; Schewski, R.; Hanke, I. M.; Pietsch, M.; Ganschow, S.; Klimm, D.; Dittmar, A.; Fiedler, A.; Schroeder, T.; Bickermann, M. Czochralski-grown bulk β-Ga_2O_3 single crystals doped with mono-, di-, tri-, and tetravalent ions. *J. Cryst. Growth* **2020**, *529*, No. 125297.

(35) Ryou, H.; Yoo, T. H.; Yoon, Y.; Lee, I. G.; Shin, M.; Cho, J.; Cho, B. J.; Hwang, W. S. Hydrothermal Synthesis and Photocatalytic

https://doi.org/10.1021/acsomega.2c05047
ACS Omega 2023, 8, 11709−11716

Property of Sn-doped β-Ga_2O_3 Nanostructure. *ECS J. Solid State Sci. Technol.* **2020**, *9*, No. 045009.
(36) Wang, C.-C.; Lee, B.-C.; Shieu, F.-S.; Shih, H. C. Characterization and photoluminescence of Sn-doped β-Ga_2O_3 nanowires formed by thermal evaporation. *Chem. Phys. Lett.* **2020**, *753*, No. 137624.
(37) Ramana, C. V.; Das, D.; Gutierrez, G.; Manciu, F. S.; Shutthanandan, V. Microstructure, chemical inhomogeneity, and electronic properties of tin-incorporated Ga_2O_3 compounds. *J. Mater. Sci.* **2022**, *57*, 11170−11188.
(38) Ramana, C. V.; Mauger, A.; Julien, C. M. Growth, characterization and performance of bulk and nanoengineered molybdenum oxides for electrochemical energy storage and conversion. *Prog. Cryst. Growth Charact. Mater.* **2021**, *67*, No. 100533.
(39) Ansari, S. M.; Sinha, B. B.; Phase, D.; Sen, D.; Sastry, P. U.; Kolekar, Y. D.; Ramana, C. V. Particle Size, Morphology, and Chemical Composition Controlled $CoFe_2O_4$ Nanoparticles with Tunable Magnetic Properties via Oleic Acid Based Solvothermal Synthesis for Application in Electronic Devices. *ACS Appl. Nano Mater.* **2019**, *2*, 1828−1843.
(40) Ramana, C.V.; Hussain, O.M.; Pinto, R.; Julien, C.M. Microstructural features of pulsed laser deposited V2O5 thin films. *Appl. Surf. Sci.* **2003**, *207*, 135−138.
(41) Roy, S.; Ramana, C. Effect of sintering temperature on the chemical bonding, electronic structure and electrical transport properties of β-$Ga_{1.9}Fe_{0.1}O_3$ compounds. *J. Mater. Sci. Technol.* **2021**, *67*, 135−144.
(42) Rao, R.; Rao, A. M.; Xu, B.; Dong, J.; Sharma, S.; Sunkara, M. K. Blueshifted Raman scattering and its correlation with the [110] growth direction in gallium oxide nanowires. *J. Appl. Phys.* **2005**, *98*, No. 094312.
(43) Fiedler, A.; Ramsteiner, M.; Galazka, Z.; Irmscher, K. Raman scattering in heavily donor doped β-Ga_2O_3. *Appl. Phys. Lett.* **2020**, *117*, 152107.
(44) Tadjer, M. J.; Freitas, J. A.; Culbertson, J. C.; Weber, M. H.; Glaser, E. R.; Mock, A. L.; Mahadik, N. A.; Schmieder, K.; Jackson, E.; Gallagher, J. C.; Feigelson, B. N.; Kuramata, A. Structural and electronic properties of Si- and Sn-doped (−201) β-Ga_2O_3 annealed in nitrogen and oxygen atmospheres. *J. Phys. D: Appl. Phys.* **2020**, *53*, 504002.
(45) Gutierrez, G.; Sundin, E. M.; Nalam, P. G.; Zade, V.; Romero, R.; Nair, A. N.; Sreenivasan, S.; Das, D.; Li, C.; Ramana, C. V. Interfacial Phase Modulation-Induced Structural Distortion, Band Gap Reduction, and Nonlinear Optical Activity in Tin-Incorporated Ga_2O_3. *J. Phys. Chem. C* **2021**, *125*, 20468−20481.
(46) Onuma, T.; Fujioka, S.; Yamaguchi, T.; Itoh, Y.; Higashiwaki, M.; Sasaki, K.; Masui, T.; Honda, T. Polarized Raman spectra in β-Ga_2O_3 single crystals. *J. Cryst. Growth* **2014**, *401*, 330−333.
(47) Leonardy, A.; Hung, W.-Z.; Tsai, D.-S.; Chou, C.-C.; Huang, Y.-S. Structural Features of SnO_2 Nanowires and Raman Spectroscopy Analysis. *Cryst. Growth Des.* **2009**, *9*, 3958−3963.
(48) Choi, E.; Lee, D.; Shin, H.-J.; Kim, N.; Valladares, L. D. L. S.; Seo, J. Role of Oxygen Vacancy Sites on the Temperature-Dependent Photoluminescence of SnO_2 Nanowires. *J. Phys. Chem. C* **2021**, *125*, 14974−14978.
(49) Zhao, X.; Wu, Z.; Guo, D.; Cui, W.; Li, P.; An, Y.; Li, L.; Tang, W. Growth and characterization of α-phase $Ga_{2-x}Sn_xO_3$ thin films for solar-blind ultraviolet applications. *Semicond. Sci. Technol.* **2016**, *31*, No. 065010.
(50) Scott, J. F. Raman Spectrum of SnO_2. *J. Chem. Phys.* **1970**, *53*, 852−853.
(51) Beattie, I. R.; Gilson, T. R. Oxide phonon spectra. *J. Chem. Soc. A* **1969**, 2322−2327.
(52) Yao, Y.; Ishikawa, Y.; Sugawara, Y. X-ray diffraction and Raman characterization of β-Ga_2O_3 single crystal grown by edge-defined film-fed growth method. *J. Appl. Phys.* **2019**, *126*, 205106.
(53) Zhang, K.; Xu, Z.; Zhang, S.; Wang, H.; Cheng, H.; Hao, J.; Wu, J.; Fang, F. Raman and photoluminescence properties of un−/ion-doped β-Ga_2O_3 single-crystals prepared by edge-defined film-fed growth method. *Phys. B* **2021**, *600*, No. 412624.
(54) Wang, X.; Chen, Z.; Zhang, F.; Saito, K.; Tanaka, T.; Nishio, M.; Guo, Q. Temperature dependence of Raman scattering in β-$(AlGa)_2O_3$ thin films. *AIP Adv.* **2016**, *6*, No. 015111.

https://doi.org/10.1021/acsomega.2c05047
ACS Omega 2023, 8, 11709−11716